nature communications

Article

https://doi.org/10.1038/s41467-024-53957-0

Self-healing electronic skin with high fracture strength and toughness

Received: 16 December 2023

Accepted: 28 October 2024

Published online: 11 November 2024

Check for updates

Jaehoon Jung[1], Sunwoo Lee[1], Hyunjun Kim[2], Wonbeom Lee[1], Jooyeun Chong[1], Insang You[3] ✉ & Jiheong Kang[2] ✉

Human skin is essential for perception, encompassing haptic, thermal, proprioceptive, and pain-sensing functions through ion movement. Additionally, it is mechanically resilient and self-healing for protection. Inspired by these unique properties, researchers have attempted to develop stretchable, self-healing sensors based on ion dynamics. However, most self-healing sensors reported to date suffer from low fracture strength and toughness. In this work, we present an ion-based self-healing electronic skin with exceptionally high fracture strength and toughness. We enhanced self-healing polymers and ionic conductors by introducing two types of orthogonal dynamic crosslinking bonds: dynamic aromatic disulfide bonds and 2-ureido-4-pyrimidone moieties. These dynamic bonds provide autonomous self-healing and high mechanical toughness even in the presence of ionic liquids. As a result, our self-healing polymer and self-healing ionic conductor exhibit remarkable stretchability (700%, 850%), fracture strength (34 MPa, 30 MPa), and toughness (78.5 MJ/m^3, 87.3 MJ/m^3), the highest values reported among self-healing ionic conductors to date. Using our materials, we developed various fully self-healing sensors and a soft gripper capable of autonomously recovering from mechanical damage. By integrating these components, we created a comprehensive self-healing electronic skin suitable for soft robotics applications.

The human skin forms an integral part of the human body. The skin is not merely an external protective barrier; it is equipped with a highly sophisticated somatosensory system based on ion movements[1–5]. This system endows the skin with the ability to detect and interpret various stimuli, including temperature, pressure, and pain. Furthermore, the skin possesses remarkable mechanical robustness and even self-healing capability, which can autonomously restore the skin's inherent functions when damage is applied.

Researchers have increasingly focused on the development of stretchable, self-healing sensors that mimic the remarkable properties of human skin[6–9]. These stretchable and self-healing sensing materials are fabricated by incorporating either electrically conductive or ionically conductive components into a self-healing polymer matrix. Self-healing capabilities could enhance the durability and lifetime of the sensors, while the electrical characteristics of the conductive fillers enable the detection of various stimuli.

Among the numerous materials for self-healing sensors, self-healing ionogels are excellent candidates[10–16]. Self-healing ionogels—that is, self-healing polymer networks swollen with ionic liquids (ILs)—have been extensively studied as ionic conductors for soft self-healing electronics due to their humidity insensitiveness, non-volatility, mechanical stretchability, and excellent electrochemical properties. They have been successfully used as a sensing layer for self-healing mechanical sensors, including pressure, strain, and shear sensors, as well as temperature sensors. Additionally, they have been utilized as electrodes in stretchable light-emitting capacitors (LEC).

[1]Department of Materials Science and Engineering, Korea Advanced Institute of Science and Technology (KAIST), Daejeon 34141, Republic of Korea. [2]Department of Chemistry, Seoul National University, Seoul 08826, Republic of Korea. [3]Department of Chemistry, University of Waterloo, 200 University Ave W., Waterloo, Ontario, ON N3L3G1, Canada. ✉e-mail: iyou@uwaterloo.ca; jiheongkang@snu.ac.kr

Nevertheless, if ionic conductors possess weak mechanical properties, they may experience permanent dimensional changes (plastic deformation) during repeated sensor operations. Such changes significantly impede accurate sensing. Therefore, improving the mechanical robustness of self-healing ionic conductors is very important for electronic skin. However, reported self-healing ionic conductors have low mechanical properties for the following reasons. The intrinsic self-healing capability of self-healing polymers is typically achieved by incorporating dynamic supramolecular interactions, such as hydrogen bonding, π- π interactions, ionic interactions, and metal-ligand coordination, into low T_g polymer matrices[17,18]. Due to their composition of dynamic bonds with weak bindings, most self-healing polymers exhibit low mechanical properties. Fortunately, several studies have been reported to design and synthesize tough, self-healing polymers trying to solve the trade-off relationship between self-healing capabilities and the mechanical properties of materials[19–23]. However, the self-healing ionic conductors designed for stretchable self-healing sensors exhibit significantly weaker mechanical properties when compared to their original self-healing polymers. This is attributed to the disruptive nature of ionic liquid on the dynamic bonds. For these reasons, no studies have developed an approach for simultaneously realizing stretchable, mechanically tough, and self-healing ionic conductors for stretchable self-healing sensors to the best of our knowledge.

Here, we report a design of a self-healing polymer and ionic conductor, possessing exceptionally ultra-high fracture strength and toughness, for stretchable self-healing sensors. The designed polymer contains two types of dynamic bonds in its polycaprolactone (PCL) main polymer chain, which is known to be biocompatible: dynamic aromatic disulfide bonds (DS) and 2-ureido-4-pyrimidone (UPy) moieties, having the role of autonomous self-healing and high mechanical toughness, respectively. DS was selected to enable efficient self-healing at room temperature through main chain shuffling. Among various self-healing moieties, DS moieties are particularly appealing due to their capability of facilitating relatively faster self-healing at room temperature through efficient disulfide metathesis[24–26]. Next, UPy units were introduced as additional dynamic bonds in polymer design to enhance the mechanical properties. The UPy moieties impart good elasticity and fracture toughness by crosslinking the polymer chains through quadruple hydrogen bonding[27,28]. Significantly, due to the formation of strong bonds between UPy units, even when ionic liquids are integrated into the polymer matrix, the robust bonding between UPy units is not broken. Consequently, these UPy moieties ensure that ionic conductors maintain their robust mechanical properties in comparison to their original polymers. However, if UPy bonds are solely introduced as dynamic bonds in the polymer chain, self-healing cannot be achieved in polymer and ionogel due to the slow bond exchanges of UPy (Fig. 1a). In contrast, if DS bonds are solely employed as dynamic bonds, the self-healing polymer (SHP) exhibit weak mechanical properties due to the low bonding strength between DS units (Fig. 1b). Moreover, when ionic liquid is added to SHP, the ionic liquid disrupts the polymer interaction resulting in significantly weakened mechanical toughness (Fig. 1b). Only when both dynamic bonds are used together, ionic conductor can achieve ultra-high toughness and self-healing property simultaneously (Fig. 1c). Interestingly, all components of PCL, DS, and UPy in our polymer design are easily aligned and further aggregated during stretching. As a result, this can enhance the fracture strength through strain-induced aggregation. As a result, our self-healing ionic conductor (SHIC) shows high stretchability (850%), high fracture strength (30 MPa), and high toughness (87.3 MJ/m^3). To the best of our knowledge, our SHIC shows the highest mechanical properties among reported self-healing ionogels.

Using our SHP and SHIC, we uniquely demonstrate tough, self-healing electronic skin and a soft gripper for somatosensitive soft robots. Due to their excellent mechanical, sensing, and self-healing properties, these soft robots can operate effectively for extended periods, even in dynamic environments.

Results

Design and synthesis of tough, self-healing polymer and ionic conductor

To impart enhanced toughness and self-healing properties to our polymers and ionic conductors, we designed materials characterized by two distinct types of dynamic bonds: a dynamic covalent bond based on aromatic disulfide (DS) and a quadruple hydrogen bond originating from ureido-pyrimidinone (UPy) (Fig. 2a). Polycaprolactone (PCL) was selected as the hydrophilic polymer backbone to ensure miscibility with ionic liquids. We synthesized a series of thermoplastic polyurethane polymers via one-pot polycondensation reactions, utilizing varying ratios of DS and UPy moieties as chain extenders (SHP-1, SHP-2, and SHP-3) (Supplementary Figs. 1, 2). SHP-1 and SHP-2 are PCL-$DS_{0.6}$-$UPy_{0.4}$ and PCL-$DS_{0.8}$-$UPy_{0.2}$, respectively (Supplementary Fig. 1). SHP-3 is PCL-DS homopolymer without UPy moieties (Supplementary Fig. 2). All polymers and materials that make up polymers are characterized by Nuclear Magnetic Resonance (NMR) and Gel Permeation Chromatography (GPC) (Supplementary Figs. 3–5).

All SHP polymers are well dissolved in *N*,*N*-dimethylacetamide. Solutions are casted on Teflon substrate and transparent free-standing films are obtained after solvent evaporation and subsequent thermal annealing at 110 °C in a vacuum. All polymer films could be stretched to more than 6 times their original length at a strain rate of 1000%/min (Fig. 2b). When polymers are synthesized only with aromatic DS moieties as chain extenders, the resulting film (SHP-3) is highly stretchable and autonomously self-healable but mechanically very weak (Fig. 2b). As UPy contents increase, mechanical strength and toughness are dramatically enhanced (Fig. 2b–d and Supplementary Figs. 6, 7). Notably, the mechanical strength and toughness of SHP-1, having 40% UPy contents in chain extenders, reached 34 MPa and 78.5 MJ/m^3, respectively (Fig. 2c, d).

Self-healing ionic conductors (SHIC) are created by incorporating 1-ethyl-3-methylimidazolium bis(trifluoromethylsulfonyl)imide (EMIM TFSI) ILs into SHP, as depicted in Fig. 2a. As previously discussed, ILs act as plasticizers within the polymer matrix, affecting the dynamic crosslinking bonds (Fig. 1b). Consequently, most previously reported SHICs have shown mechanical weakness and excessive viscoelasticity.

To our surprise, SHIC-1 exhibited remarkable mechanical properties. Despite containing 5 wt% of ILs, the fracture strength of SHIC-1 almost matches that of SHP-1 (Fig. 2c). Figure 2c, d demonstrate that the UPy content in the polymers is crucial for maintaining mechanical properties after introducing ILs. In contrast, SHIC-3, which relies solely on DS as chain extenders, showed mechanical instability due to the disruption of crosslinking by ILs (Fig. 2d and Supplementary Fig. 6).

These remarkable findings are attributed to the multivalent effect of quadruple hydrogen bonding, which enhances the stability of UPy-UPy crosslinking bonds, even in the presence of ILs. Upon measuring the rheological data of self-healing materials, it was observed that SHP-3, which lacks UPy content, exhibited a crossover point at lower frequencies with the addition of ionic liquid. In contrast, SHP-1 did not display any crossover point, even with the addition of ionic liquid (Supplementary Fig. 7). Additionally, differential scanning calorimetry (DSC) measurements revealed that SHP-1, which contains the UPy moiety, exhibited a significantly lower reduction in T_g upon the addition of ionic liquid compared to SHP-3 (Supplementary Fig. 8). These measurements indicate that the strong hydrogen bonding of the UPy moieties allow SHIC-1 to maintain its chain rigidity almost unchanged, even with the addition of ionic liquid. Consequently, SHIC-1 exhibits exceptionally high toughness, superior elasticity, and notch-insensitive high stretchability (Supplementary Figs. 9–11). This strength and toughness are evident in

https://doi.org/10.1038/s41467-024-53957-0

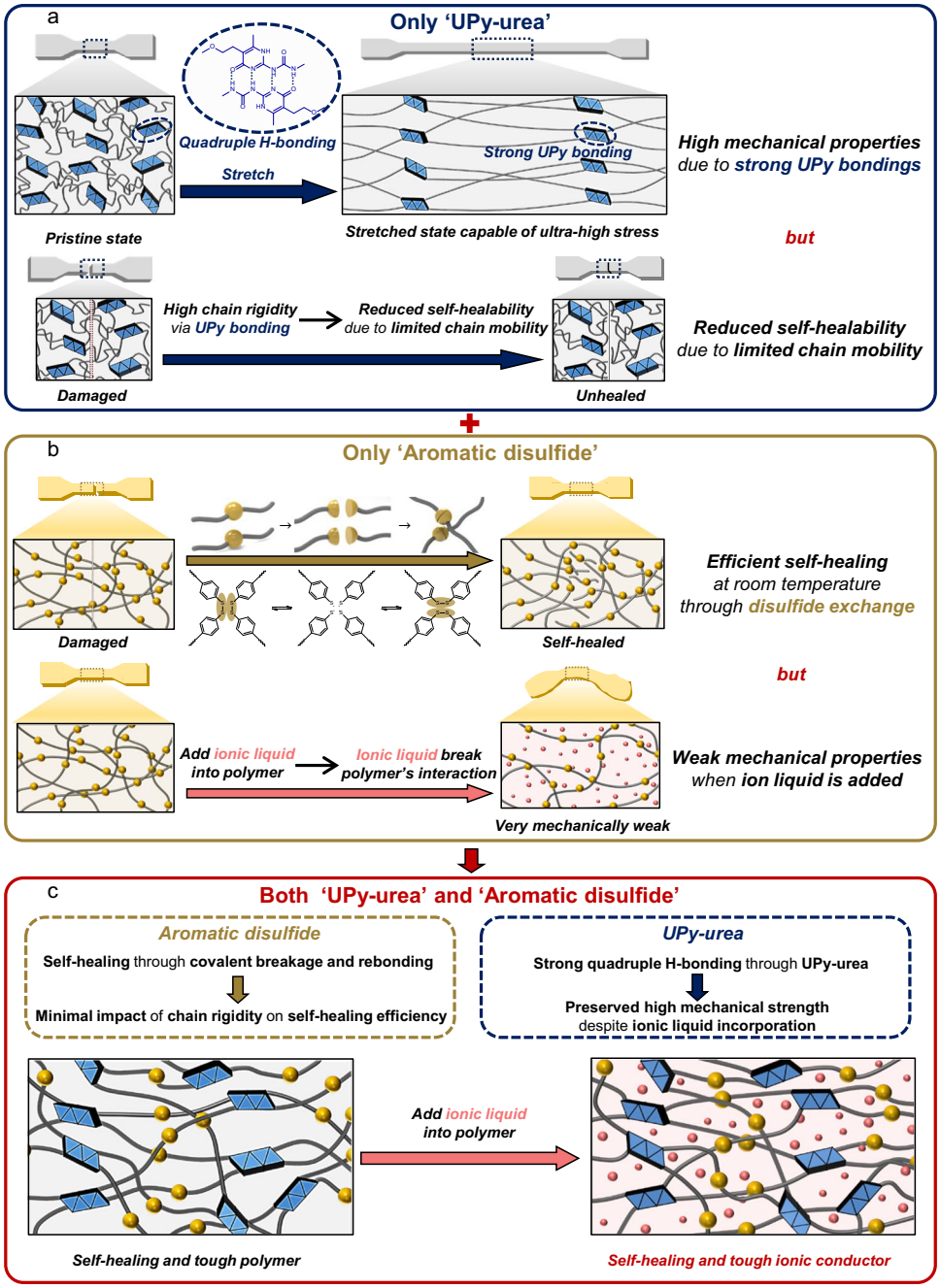

Fig. 1 | Design of tough, self-healable ionic conductor. a Schematic illustration of a polymer featuring UPy-urea as the sole dynamic bond. When using UPy-urea as the sole dynamic bond in a polymer, the strong hydrogen bonds between UPy-urea units result in high mechanical properties. However, due to the strong hydrogen bonds, the chain mobility is significantly reduced, greatly diminishing the polymer's self-healing ability. **b** Schematic illustration of a polymer featuring aromatic disulfide as the sole dynamic bond. When using aromatic disulfide as the sole dynamic bond in a polymer, the polymer enables efficient self-healing at room temperature through disulfide exchange. However, when an ionic liquid is added to the polymer as an ionic conductor, it disrupts the interaction between polymer chains, resulting in significantly lower mechanical properties compared to the polymer alone. **c** Schematic illustration of a polymer featuring UPy-urea and aromatic disulfide as the dynamic bonds. In the case of disulfide exchange, self-healing occurs through the breaking and reforming of dynamic covalent bonds, which makes the impact of chain rigidity on self-healing efficiency relatively low. Additionally, due to the strong quadruple hydrogen bonding between UPy-urea units, the ionic liquid cannot disrupt these strong bonds, allowing the ionic conductor to maintain its high mechanical properties even with the addition of the ionic liquid. Consequently, when using both UPy-urea and aromatic disulfide as the dynamic bonds in a polymer, it is possible to design an ionic conductor that possesses high mechanical properties and enables self-healing at room temperature.

Fig. 2e, where a small notched SHIC-1 film (0.001 kg) was able to lift a 6 kg dumbbell, 6000 times heavier than the film's weight. Furthermore, even with the addition of 30 wt% ionic liquid to SHP-1, sufficient to achieve high ionic conductivity (2.30×10^{-4} S/cm) for electrode applications, it was observed that SHIC-1 (30 wt% EMIM TFSI) maintains a high toughness of 47.2 MJ/m^3 (Supplementary Fig. 12).

However, it was observed that a very high UPy ratio (PCL-$S_{0.4}$-$U_{0.6}$) or the use of an alkyl group instead of a disulfide moiety (PCL-$H_{0.6}$-$U_{0.4}$) resulted in significantly low self-healing efficiency (Supplementary Fig 13). Complete self-healing at room temperature was only achievable with an appropriate ratio of UPy and aromatic disulfide (SHP-1) (Fig. 2f and Supplementary Fig. 14). Through this molecular-level polymer

https://doi.org/10.1038/s41467-024-53957-0

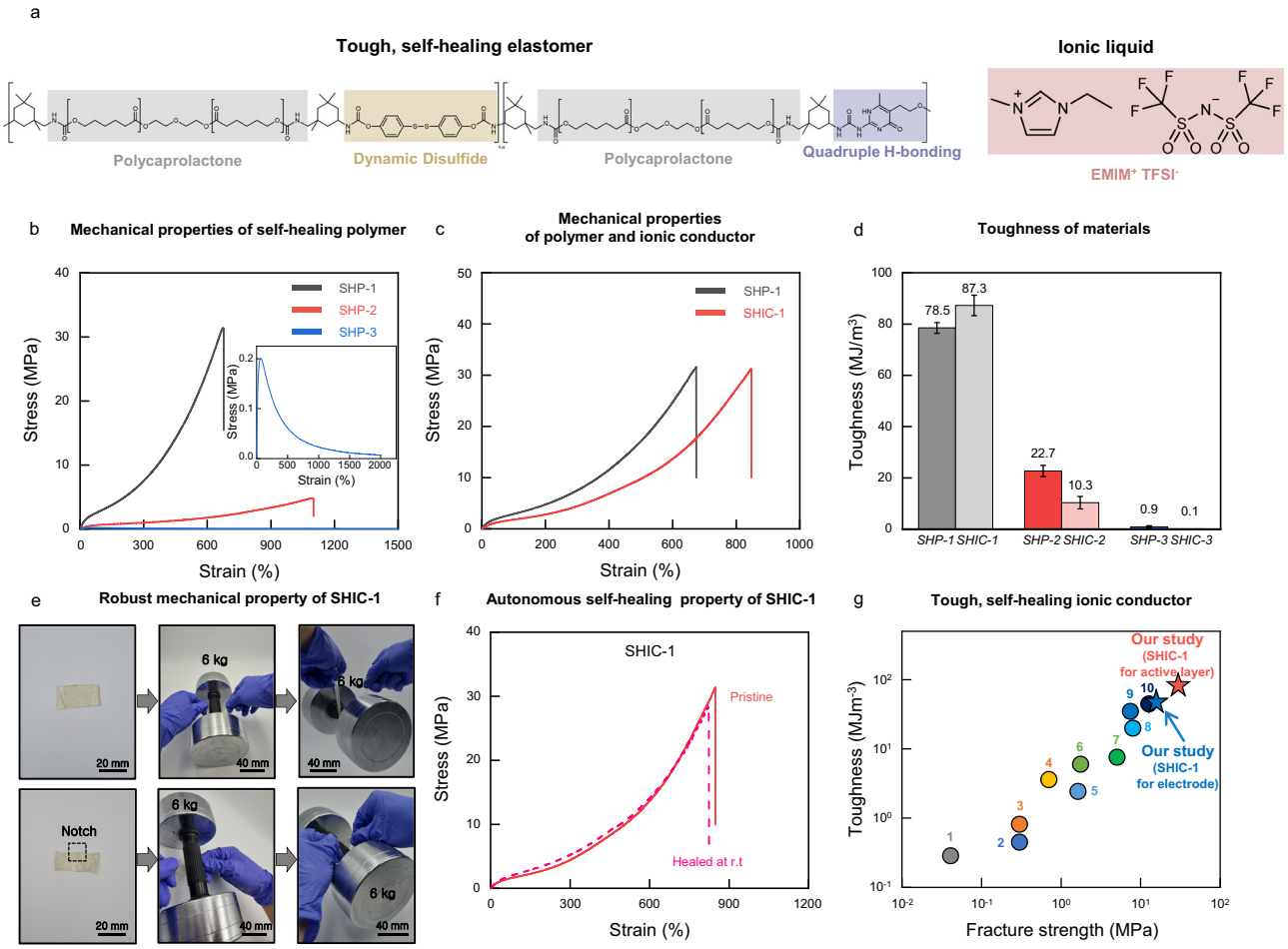

Fig. 2 | Tough, self-healing polymers and ionic conductors. a Design of the tough, self-healing elastomer and ionic conductor. **b** Stress–strain curves of the dog bone prepared with SHP-1 (black), SHP-2 (red), and SHP-3 (blue) with a sample width of 2 mm, a thickness of 2 mm, and a length of 10 mm at a loading rate of 100 mm/min. **c** Stress–strain curves of the dog bone prepared with SHP-1 (black) and SHIC-1 (red). **d** Graph comparing the toughness of materials. The data plotted represents the mean and standard deviation ($n = 3$, n means number of independent experiments). **e** Images of lifting 6 kg dumbbell using SHIC-1 film and SHIC-1 film with notch. **f** Stress–strain curves of SHIC-1 dog bone healed at room temperature. **g** A comparison of this work to recent work in self-healing ionic conductors. (Supplementary Table 1).

design, our SHIC-1 shows autonomous self-healability even with the highest fracture strength and toughness among the reported self-healing ionic conductor (Fig. 2h and Supplementary Table 1).

Fabrication of self-healable sensors for electronic skin

In physiology, the somatosensory system comprises haptic, thermal perception, proprioception, and pain sensing. By mimicking the human somatosensory system, we have developed multiple fully self-healable sensors utilizing our designed self-healing materials. Among them, the most vulnerable part of these sensors is the self-healing multimodal sensors, since they directly interact with the target object. Among various sensor structures, we adopted a recently developed stretchable multimodal sensor which is capable of independent strain and temperature detection based on ion relaxation dynamics[29]. The functionality of multimodal sensors is not affected by the dimensions of the sensor structure. This makes them highly suitable for the self-healing process, as the dimensions might slightly change during mechanical damage and self-healing.

The multimodal sensor consists of a self-healing ion conducting film (SHIC) sandwiched between two electrodes made of self-healing polymer HU-PDMS with Ag flakes (Fig. 3a and Supplementary Figs. 15, 16). HU-PDMS, being immiscible with ILs, acts as an electrode binder to prevent ionic liquid diffusion from SHIC (Supplementary Fig. 17). And for the active layer, SHIC-1 with 5 wt% EMIM TFSI, which exhibits the highest temperature sensitivity, was selected (Supplementary Fig. 18). The ion conductor's parameters (bulk resistance and geometrical capacitance) are measured at different frequencies, and relaxation time (τ) and normalized capacitance (C/C_o) are used as variables. This approach enables strain-insensitive temperature sensitivity within the body temperature range (30 - 60 °C), regardless of large deformation ($\varepsilon = 0$–50%) (Supplementary Figs. 19, 20). Similarly, normalized capacitance shows reliable temperature-insensitive strain sensitivity ($\varepsilon = 0$–50%) (Supplementary Figs. 21, 22). Thus, this multimodality enables both sensing functions within a simple and single structure, eliminating the need for additional setup to decouple thermal sensitivity from mechanical sensitivity.

The high mechanical toughness and autonomous self-healing capabilities of SHIC-1 enable operation resilience after mechanical damage, making this design advantageous as a self-healable multimodal sensor. Interestingly, due to the chemical incompatibility between the active layer (SHIC-1) and the electrode layer (HU-PDMS), healing is only activated when they align properly (Fig. 3a), inducing autonomous alignment during the healing process. Moreover, since the geometrical properties (d and A) are canceled out in the variables (τ and C/C_o) of the multimodal sensor, the system ensures consistent outputs even after damaging and healing processes (Fig. 3a). Figure 3b shows the self-healing process of the damaged ionic and electronic conductor components of the sensor. The healing process occurs spontaneously at

https://doi.org/10.1038/s41467-024-53957-0

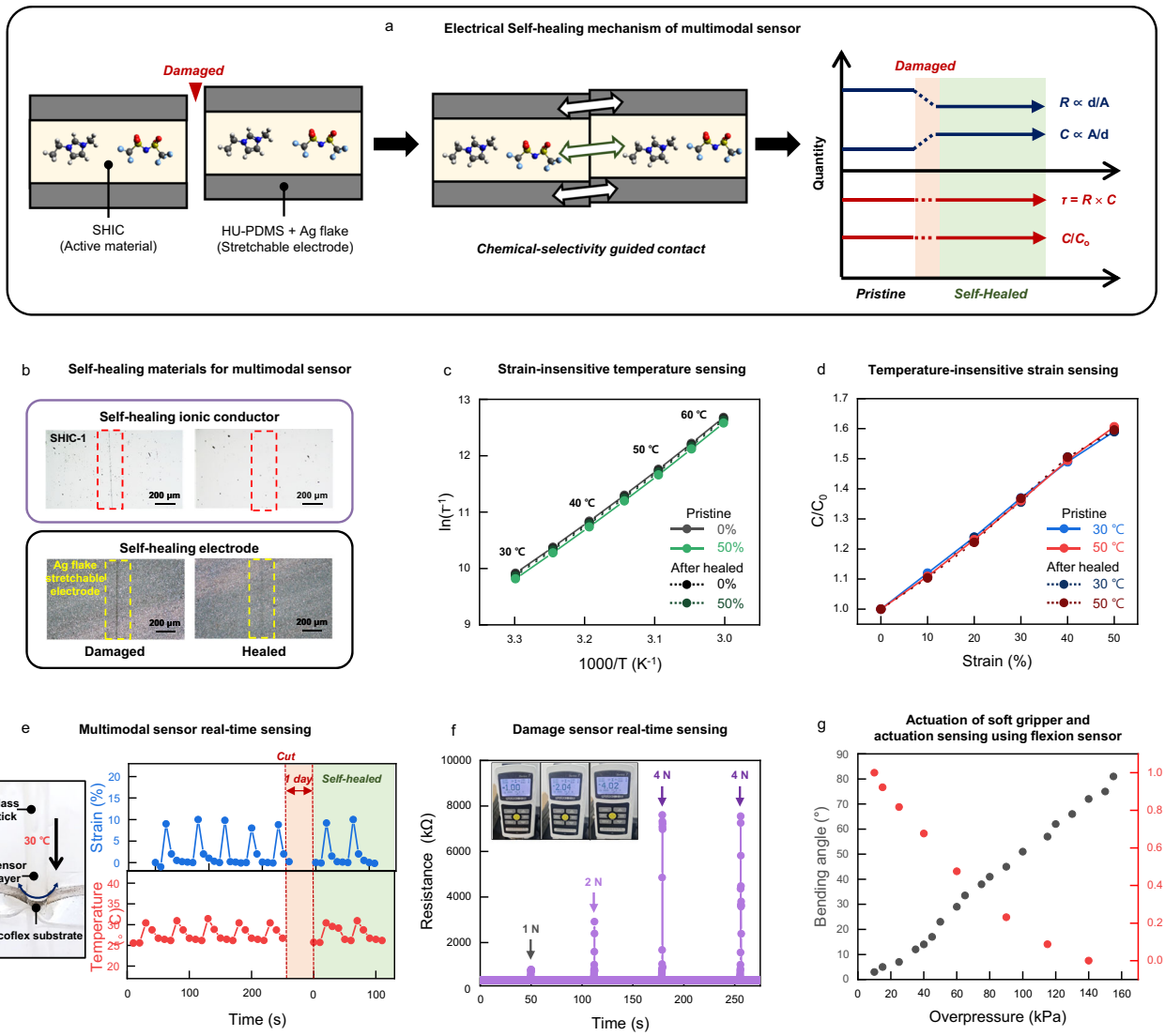

Fig. 3 | Self-healable artificial sensors. a Schematic illustration of an electrical self-healing mechanism of a multimodal sensor. **b** Optical microscope images of the damaged and healed ionic conductor and electrode film showing the disappearance of the scar after healing at room temperature for 2 days. **c** Changes of ln (τ^{-1}) with respect to T^{-1} (T, temperature) at various tensile strains (ε). The solid lines show pristine sample data, and the dotted lines show self-healed sample data. ln (τ^{-1}) is insensitive to strains. **d** Changes of C/C_0 with respect to tensile strain at different temperatures. The solid lines show pristine sample data, and the dotted lines show self-healed sample data. C/C_0 is insensitive to temperature. **e** Camera image showing the self-healing multimodal sensor pressed by a hot glass stick. This self-healing multimodal sensor shows reliable multimodal sensing ability and self-healing ability. **f** Plot of electrical characteristics of self-healing damage sensor as a function of time while undergoing damage of different mechanical strength (1–4 N). **g** Changes of bending angle of the soft gripper (black dots) and R/R_0 of the flexion sensor (red dots) as a function of overpressure. The soft gripper made of SHP-1 and SHP-2 can be actuated well after perforation.

room temperature without additional treatment, and the disappeared scar is clearly observable. Figure 3c, d demonstrate the temperature and strain responsivity of the multimodal sensor after healing, with negligible deviation compared to the pristine state (see Supplementary Fig. 23). The real-time responses of the multimodal sensor are tested by applying strain with a warm glass stick (Fig. 3e). The sensor shows reliable and consistent responses to mechanical and thermal stimulation even after cutting and healing processes, without signal distortion.

Another self-healing sensor is the damage sensor. The damage sensor is made from SHIC-1 with 30 wt% EMIM TFSI. The damaged sensor exhibits real-time responsivity to mechanical damage by sharp objects (Fig. 3f). Upon damage, a large increase in resistance is observed, and it quickly recovers to its original state, showing consistent responses[30]. Unlike stretchable electronic conductors with inorganic conductive fillers, the ion conductor requires only small amounts of ionic molecules to form a conductive path in the polymer, enabling immediate healing after damage (Supplementary Fig. 24). In addition, their high toughness and elasticity enable the rapid reformation of interface contact in the damaged area.

The final self-healing sensor is the flexion sensor, responsible for perceiving actuation. The flexion sensor is composed of conductive nickel particles embedded in SHP-3[31]. An experiment was conducted by applying strain to the sensor and measuring the change in resistance (Supplementary Fig. 25). At low levels of strain, micro-Ni particles of the flexion sensor form a conductive network, leading to a sharp decrease in resistance[32]. Therefore, when the flexion sensor is positioned on the outside of the gripper, a small strain is applied to the gripper during actuation, resulting in a change in resistance. As a result, by measuring resistance, the sensor can provide feedback to enable reliable operation of pneumatic actuators. Figure 3g illustrates the flexion sensor's response to increased small strain applied to the actuator, leading to an increase in bending angle and a decrease in resistance due to small

https://doi.org/10.1038/s41467-024-53957-0

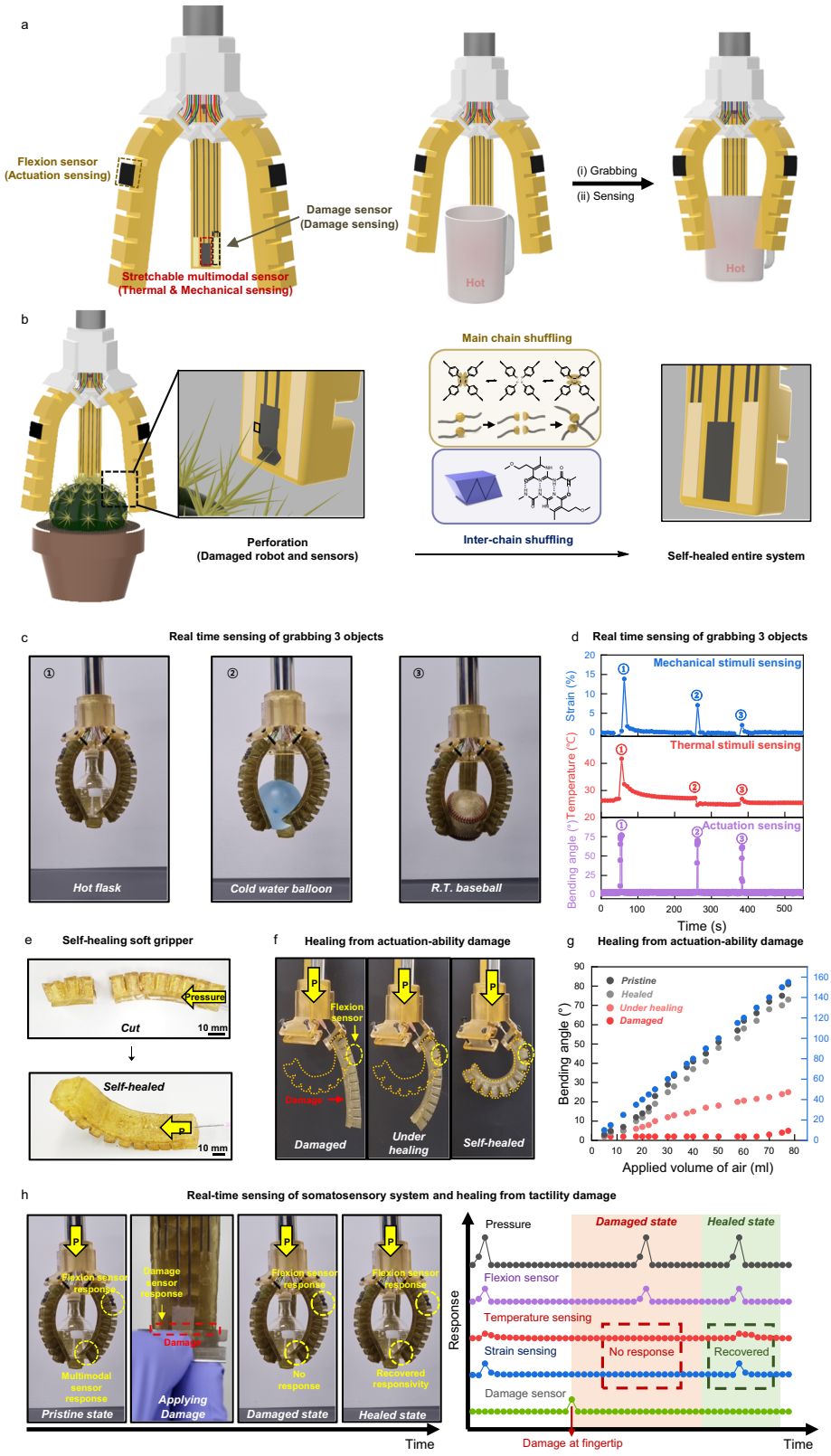

strain. Additionally, the flexion sensor demonstrated reliable resistance changes corresponding to the bending angle, even with repeated actuations of the gripper (Supplementary Fig. 26).

Self-healable soft gripper with self-healable sensors

Next, we developed a soft pneumatic actuator for soft gripper applications (Fig. 4a)[33,34]. The prototype was fabricated using solely SHP. The actuator consisted of 11 inflatable air chambers made of SHP-2 (modulus: 0.39 MPa) produced through thermal molding. To achieve a large bending angle, the bottom layers were made with SHP-1 (modulus: 3.5 MPa) (Supplementary Fig. 27). The 11 air chambers were embedded onto the bottom layer at ambient conditions, and the self-healing process ensured robust interface adhesions between the chambers and the bottom layer. The resulting gripper exhibited a

Fig. 4 | Demonstration of tough, self-healable, and somatosensitive soft robot. **a** Schematic illustration of the robust, self-healing soft robot with a stretchable multimodal sensor, damage sensor, and flexion sensor. All components of the soft robot are constructed from durable, self-healing elastomer, along with resilient and self-healing conductors and ionic conductors. **b** Schematic illustration of the autonomous restoration of actuating and sensing functions. Thanks to the inherent high toughness and self-healing properties of the soft robot's materials, it is capable of automatic mechanical and electrical self-repair, facilitating the restoration of actuating and sensing functions. **c** Photographs of a soft robot grabbing three objects. **d** Real time sensing of grabbing three objects. Multimodal sensor and flexion sensor recognized mechanical stimuli, thermal stimuli from target objects and actuation of grippers accurately. **e** Photographs of the self-healing soft gripper. After cutting the gripper in half, the grippers were attached to each other. After some time, a self-healed gripper could be actuated well. **f** Photographs of self-healing from actuation-ability damage. After applying the notch to the gripper, we measured the maximum actuation capability of the soft gripper over time. The yellow-dotted illustration shows the maximum actuation capability of a pristine soft gripper. **g** Graph comparing changes of bending angle with respect to the applied volume of air (Pristine gripper, self-healed gripper, gripper under healing, and damaged gripper). **h** Photographs and graph of real-time sensing of the somatosensory system and healing from tactility damage.

substantial bending angle (>81°) and the ability to grab various objects (Supplementary Figs. 28, 29).

To impart sensing abilities to self-healing gripper, the self-healing multimodal sensor and two damage sensors are located at the fingertip and the flexion sensor is placed at the back of the finger (Fig. 4a and Supplementary Fig. 30). When the soft robot grabs the unknown object, the soft robot can obtain information about grabbed object through the multimodal sensor (Fig. 4a, Supplementary Figs. 31, 32, and Supplementary Movies 1, 2). Additionally, the flexion sensor provides accurate bending angle data, enabling more precise operation (Supplementary Movie 3). Furthermore, when the soft robot is damaged, the DS bonds enable a rapid self-healing process through main chain shuffling via disulfide metathesis between polymer chains, occurring at room temperature. Meanwhile, the UPy moieties impart good elasticity and fracture toughness by crosslinking the polymer chains through quadruple hydrogen bonding (Fig. 4b). Consequently, the designed soft robot exhibits high durability and resilience, ensuring the reliable operation even under challenging environments. In Fig. 4c, the soft gripper is shown, consisting of three soft actuators acting as fingers. These self-healing sensors allow the gripper to perceive mechanical and thermal stimuli from the target object and sense the bending motion of the soft gripper itself while grasping various objects (Fig. 4d).

The self-healability of the somatosensitive soft gripper was then tested. Since the gripper is made entirely of SHP, even a complete cut could be healed at room temperature (Fig. 4e). There are two types of malfunctions due to damage: (1) disabled actuation and (2) disabled sensation. Figure 4f illustrates the first case, where the pressure responsivity of the damaged actuator is disabled. Damage, especially penetration, prevents the actuator from responding to applied pressure due to air leakage through the scar. As healing progresses and the scar size decreases, the actuator partially recovers its responsivity. After sufficient time for the self-healing process, the scar fully heals, and the original actuating performance is restored. The entire process of damaging and healing can be monitored by the flexion sensor, which fulfills its role akin to biological systems (Fig. 4g). By comparing the applied volume of air with the flexion sensor's responsivity, it is possible to determine if the flexion sensor is operating normally and to track the progress of self-healing. Figure 4h demonstrates the second case of malfunction caused by damage affecting tactile sensation. In the pristine state, both the flexion sensor and multimodal sensor (temperature and strain sensing) respond well during grasping behavior with applied pressure, as seen in the early period of Fig. 4h. However, when damage is applied to the fingertip using a sharp object to simulate a disabled sensation, the damage sensor instantly senses the damage, as depicted in the initial period of the damaged state in Fig. 4h. Due to electrical disconnection at the fingertip region, the multimodal sensor loses its function, resulting in no responsivity to temperature and strain sensing, even though the object contacts with the gripper. Information from the flexion sensor indicates that the gripper's actuation is still functioning well in the damaged state, suggesting that the damage did not cause penetration of the body. After some time, the self-healing of the multimodal sensor enables the recovery of temperature and strain sensing under actuation. Thus, it is confirmed that self-healing is applied not only to the actuator body itself but also to the artificial somatosensory system. Particularly in a self-healing device, such a self-diagnosis system is indispensable for confirming the successful functioning of the healing process.

Discussion

By incorporating two types of dynamic bonds into the polymer system, we have developed an elastomer and ionic conductor that possesses both excellent mechanical properties and efficient self-healing capability at room temperature. The self-healing capability was imparted by introducing an aromatic disulfide moiety, while a UPy moiety was added to maintain strong mechanical properties even with the incorporation of an ionic liquid. Only when both dynamic bonds are used together in the proper ratio can the ionic conductor achieve ultra-high toughness and self-healing properties simultaneously. We have developed various sensors for fully self-healable electronic skin and actuators, which can be applied to self-healing somatosensitive soft robotic systems. We believe that our material design strategy will significantly advance the progress of self-healing soft electronics.

Methods

Materials

Poly(caprolactone) diol (Mn = 1000 $gmol^{-1}$) was purchased from Human Juren Chemical Hitechnology (China). Isophorone diisocyanate (98%), 1-ethyl-3-methylimidazolium bis(trifluoromethylsulfonyl)imide (EMIM TFSI), 3-ethyl-1-methyl-1H-imidazol-3-ium Bis(fluorosulfonyl) azanide (EMIM FSI), and bis(4-hydroxyphenyl) disulfide (98%) were purchased from TCI (Japan). *N*,*N*′-dimethylacetamide (DMAc, 99.8%), guanidine carbonate salt (99%), absolute ethanol, triethylamine (99.5%), α-acetylbutyrolactone (99%), Ag flake (99.9%), hexamethylene diisocyanate (99%), Dichloromethane, 4-benzoylbenzoic acid (99%), poly(ethylene glycol) (Mn = 2000 $gmol^{-1}$), 4-(Dimethylamino)pyridine (99%), EDC•HCl, Hydrochloric acid, Magnesium sulfate, 4,4′-Methylenebis(phenyl isocyanate) (98%), methanol (anhydrous, 99%), chloroform (anhydrous, 99%), 4-methyl-2-pentanone (99%), and dibutyltin dilaurate (DBTDL, 95%) were purchased from Sigma-Aldrich (USA). Aminopropyl-terminated polydimethylsiloxane (aminopropyl terminated PDMS) (Mn = 1000 $gmol^{-1}$) was purchased from Gelest (USA). All materials were used without purification.

Synthesis of 2-amino-5-(2-hydroxyethyl)−6-methylpyrimidin-4(3H)-one (UPy)

UPy was prepared according to the published procedures[35]. A mixture of α-acetylbutyrolactone (2.2 mL, 20 mmol) and guanidine carbonate (1.5 g, 20 mmol) was refluxed with absolute ethanol (20 mL) in the presence of triethylamine (5.5 mL, 40 mmol) for 1 h; the mixture became clear, then precipitated a pale yellow solid. The reaction was continued for 4 h. The precipitate was filtered, washed with ethanol and dried under vacuum to afford 1.16 g of UPy (69%) as a white solid.

Synthesis of pre-polymer for SHP

Poly(caprolactone) diol (20 g, 20 mmol) was placed in a dried 3-neck round-bottom flask equipped with a mechanical stirrer and heated in

an oil bath at 100 °C under vacuum for 1 h under Ar atmosphere to remove any moisture. And then it cooled to 70 °C. Isophorone diisocyanate (8.892 g, 40 mmol) and DBTDL (20 μl) dissolved in DMAc (10 ml) were added to the reaction vessel, with stirring continued for 2 h under Ar atmosphere.

SHP-1. After the pre-polymer had been synthesized, the reactor was cooled to 65 °C and bis(4-hydroxyphenyl) disulfide (3 g, 12 mmol), UPy (1.35344 g, 8 mmol), and triethylamine (20 μl) dissolved in DMAc (20 ml) were added dropwise to the reactor. The reactor was cooled to 40 °C and the reaction was continued for under Ar atmosphere. And then the reactor was heated to 85 °C, with stirring continued for overnight under Ar atmosphere.

SHP-2. After the pre-polymer had been synthesized, the reactor was cooled to 65 °C and bis(4-hydroxyphenyl) disulfide (4 g, 16 mmol), UPy (0.67672 g, 4 mmol), and triethylamine (20 μl) dissolved in DMAc (20 ml) were added dropwise to the reactor. The reactor was cooled to 40 °C and the reaction was continued for under Ar atmosphere. And then the reactor was heated to 85 °C, with stirring continued for overnight under Ar atmosphere.

SHP-3. After the pre-polymer had been synthesized, the reactor was cooled to RT and bis(4-hydroxyphenyl) disulfide (5 g, 20 mmol), dissolved in DMAc (20 μl) were added dropwise to the reactor. The reactor was heated to 40 °C and the reaction was continued for under Ar atmosphere. And then the reactor was heated to 85 °C, with stirring continued for overnight under Ar atmosphere.

PCL-$S_{0.4}$-$U_{0.6}$. After the pre-polymer had been synthesized, the reactor was cooled to 65 °C and bis(4-hydroxyphenyl) disulfide (2 g, 8 mmol), UPy (2.03 g, 12 mmol), and triethylamine (0.1 g) dissolved in DMAc (20 ml) were added to the reactor. The reactor was cooled to 40 °C and the reaction was continued under the Ar atmosphere. And then the reactor was heated to 85 °C, with stirring continued overnight under the Ar atmosphere. After polymers had been synthesized, the reactor were worked up by adding excess methanol. And then, the solvent was evaporated at 130 °C overnight in a vacuum oven. After SHPs was dissolved in THF, the product was washed with methanol three times.

Synthesis of HU-PDMS for self-healing electrode

After dichloromethane was placed in a dried glass vessel, the reactor was cooled to 0 °C, and triethylamine and aminopropyl terminated PDMS were added to the reactor. Then hexamethylene diisocyanate was added dropwise to the reaction vessel with stirring continued for 1 h under Ar atmosphere. After the polymer had been synthesized, the reactor was heated to room temperature and worked up by adding excess methanol. Methanol was evaporated by a rotary evaporator. After HU-PDMS was dissolved in chloroform, the product was washed with methanol three times. The product was dried at 50 °C for 3 h and further dried at 50 °C for overnight in a vacuum oven.

General measurements

^{1}H NMR spectroscopy was recorded on a 400 MHz spectrometer (Varian, USA) in deuterated solvents at room temperature. Size exclusion chromatography (SEC) was performed in *N*,*N*-dimethylformamide at 45 °C with a flow rate of 1 ml/min on an Agilent 1260 Infinity system (Santa Clara, CA). The instrument is equipped with a 1260 refractive index detector and one PSS GRAM analytical 100 Å column in series with a molar mass range 300–60,000 g mol^{-1}, two PSS GRAM analytical 10,000 Å columns in series with a molar mass range 10,000–50,000,000 g mol^{-1}. The molar masses of the polymers were calculated relative to linear polystyrene standards obtained from Agilent Technologies. Scanning Electron Microscope (SEM) image was acquired on an S-4800 (Hitachi, Japan).

Sample preparation

Preparation of SHP film. DMAc solution of SHP was cast onto a Teflon sheet and heated at 100 °C for 48 h and further dried for 24 h at 110 °C in a vacuum oven.

Preparation of SHP dog bone. SHP film was prepared using a hot-press machine (QMESYS, Korea) and pressed into Teflon molds at 130 °C and 100 bar for 5 min.

Preparation of SHIC film. SHP polymers were dissolved in DMAc (200 mg/ml) along with EMIMTFSI (5 wt%). After dissolving, the solution was degassed and cast into a surface treated glass, and evaporated at 80 °C overnight. Then the film was further dried for 12 h at 80 °C in a vacuum oven (film thickness = 100–150 μm).

Preparation of SHIC dog bone. SHIC film was prepared using a hot-press machine (QMESYS, Korea) and pressed into Teflon molds at 130 °C and 100 bar for 5 min.

Mechanical and self-healing tests

Mechanical and self-healing properties were examined with a universal testing machine (UTM) (Instron 68SC-1, USA), loaded with a 1 kN load cell, and driven at a constant crosshead speed of 1000% min^{-1} at room temperature. A 2-mm-thick dumbbell-shaped sample (IEC-540(S)), with a gauge length of 10 mm and a width of 2 mm, was cut in half with a blade and then reattached to evaluate its self-healing properties. For fracture tests, A 200-μm-thick film with a gauge length of 10 mm and a width of 40 mm was prepared. And for a notched sample, a notch of 20 mm length was made. The strain rate for the fracture test was 1000% min^{-1}. Values of all properties were determined according to data from at least three trials.

Fabrication of sensors

Self-healing stretchable electrode. HU-PDMS was dissolved in 4-methyl-2-pentanone (600 mg/ml). Then Ag flake (10 μm size) was added to HU-PDMS solution. The self-healing stretchable electrode solution was obtained through stirring for 5 min by thinky mixer.

Self-healing artificial multimodal sensor. After covering the SHIC-1 film with a PET mask, a self-healing stretchable electrode solution was dropped. Then 8 mm × 20 mm of an electrode was gained by stencil printing. After the electrode was dried at 50 °C for 3 h, the bottom surface was also printed with the same process. In this case, the area of the upper and lower overlapping electrodes is 5 mm × 10 mm, and the size of the active layer (SHIC) is the same.

Self-healing damage sensor. SHP-1 was dissolved in DMAc (250 mg/ml) along with EMIM FSI (30 wt%). After dissolving, the solution was degassed and cast into a surface treated glass, and evaporated at 80 °C overnight. Then, the film for the damaged sensor was further dried for 12 h at 80 °C in a vacuum oven (film thickness = 150–200 μm).

Self-healing flexion sensor. SHP-3 and micro-Ni powder (3:1 in weight ratio) were dissolved in Chloroform (500 mg/ml). After dissolved, the solution was degassed and cast into a surface treated glass, and evaporated at RT overnight. Then the flexion sensor was gained.

Electrical self-healing tests

Electrical self-healing properties were examined with electrochemical impedance spectroscopy (WonAtech, Korea). First, Impedance of artificial multimodal sensor was measured. Then artificial multimodal sensor was cut in half with a blade and then reattached. After some time, the impedance of cut artificial multimodal sensor was measured. Then, we compared the impedance of self-healed one and the previous one.

Self-healing soft gripper

An extensive layer of soft gripper was made of SHP-2. SHP-2 polymers were filled in Teflon mold for an extensive layer and then pressed at 130 °C for 30 min using a hot-press machine to remove any bubbles. Inextensive layer of soft gripper was made of SHP-1 in the same way as before. After inextensive layer was heated at 90 °C, two layers were attached together, and completely stuck while self-healing.

Impedance measurement

Impedance was measured on Electrochemical Impedance Spectroscopy (WonAtech, Korea). The applied AC potential was 300 mV and the frequency scanned from 1 Hz to 1 MHz. The sensor was connected to the electrochemical impedance spectroscopy by the conductive Ni tape. The sensor attached to the homemade stretcher was in contact with the rheometer (MCR302; Anton Paar, Austria). A rheometer was used to change the temperature. A homemade stretcher was used to change the strain.

Thermal and mechanical measurement

An artificial multimodal sensor for thermal and mechanical stimuli sensing was attached to the soft gripper. The measurement method was used according to published procedures[29]. Impedance was measured at two frequencies (200 Hz, 5×10^5 Hz) alternatively using Electrochemical Impedance Spectroscopy (WonAtech, Korea). The data points were obtained every 2 s. R was measured from Z_{re} at 200 Hz, and C was measured from Zim at 5×10^5 Hz. Temperature was calculated using charge relaxation time (RC) values. The strain was calculated using normalized capacitance (C/C_0).

Damage measurement

Electrical measurements of the self-healable electrodes were performed using an LCR meter (Hewlett Packard 4284a) while introducing various levels of force into the electrodes with a razor blade. The force of the razor blade on the electrode was measured by the Force Gauge Model (MARK-10, USA).

Actuation measurement

Electrical measurements of the actuation sensors were performed using an LCR meter (Hewlett Packard 4284a) while introducing various bending angles by air pressure.

Data availability

The data that support the findings of this study are available within this article and its Supplementary Information. Source data is provided as a Source Data file. Additional data were available from the corresponding author upon request. Source data are provided with this paper.

References

1. Hammock, M., Chortos, A., Tee, B. C. K., Tok, J. B. H. & Bao, Z. 25th anniversary article: the evolution of electronic skin (E-Skin): a brief history, design considerations, and recent progress. *Adv. Mater.* **25**, 5997–6038 (2013).
2. Yang, J. et al. Electronic skin: recent progress and future prospects for skin-attachable devices for health monitoring, robotics, and prosthetics. *Adv. Mater.* **31**, 1904764 (2019).
3. Lee, Y. et al. Mimiking human and biological skins for multifunctional skin electronics. *Adv. Func. Mater.* **30**, 1904523 (2019).
4. Longo, M., Azanon, E. & Haggard, P. More than skin deep: body representation beyond primary somatosensory cortex. *Neurophsychologia* **48**, 655–668 (2010).
5. McGlone, F. & Reilly, D. The cutaneous sensory system. *Neurosci. Biobehav. Rev.* **34**, 148–159 (2010).
6. Huynh, T.-P., Sonar, P. & Haick, H. Advanced materials for use in soft self-healing devices. *Adv. Mater.* **29**, 1604973 (2017).
7. Zhang, Q., Liu, L., Pan, C. & Li, Dong Review of recent achievements in self-healing conductive materials and their applications. *J. Mater. Sci.* **53**, 27–46 (2018).
8. Kang, J., Tok, J. B. H. & Bao, Z. Self-healing soft electronics. *Nat. Electron.* **2**, 144–150 (2019).
9. Khatib, M., Zohar, O. & Haick, H. Self-healing soft sensors: from material design to implementation. *Adv. Mater.* **33**, 2004190 (2021).
10. Cao, Y. et al. A transparent, self-healing, highly stretchable ionic conductor. *Adv. Mater.* **29**, 1605099 (2017).
11. Cao, Y. et al. Self-healing electronic skins for aquatic environments. *Nat. Electron.* **2**, 75–82 (2019).
12. Zhang, L. et al. Self-healing, adhesive, and highly stretchable ionogel as a strain sensor for extremely large deformation. *Small* **15**, 1804651 (2019).
13. Li, H., Xu, F., Guan, T., Li, Y. & Sun, J. Mechanically and environmentally stable triboelectric nanogenerator based on high-strength and anti-compression self-healing ionogel. *Nano Energy* **90**, 106645 (2021).
14. Xu, L. et al. A transparent, highly stretchable, solvent-resistant, recyclable multifunctional ionogel with underwater self-healing and adhesion for reliable strain sensors. *Adv. Mater.* **33**, 2105306 (2021).
15. Zhang, M. et al. Self-healing, mechanically robust, 3D printable ionogel for highly sensitive and long-term reliable ionotronics. *J. Mater. Chem. A.* **10**, 12005–12015 (2022).
16. Yang, L. et al. Mechanically robust and room temperature self-healing ionogel based on ionic liquid inhibited reversible reaction of disulfide bonds. *Adv. Sci.* **10**, 2207527 (2023).
17. Yang, Y. & Urban, M. W. Self-healing polymeric materials. *Chem. Soc. Rev.* **42**, 7446–7467 (2013).
18. Wang, S. & Urban, M. W. Self-healing polymers. *Nat. Rev. Mater.* **5**, 562–583 (2020).
19. Kang, J. et al. Tough and water-insensitive self-healing elastomer for robust electronic skin. *Adv. Mater.* **30**, 1706846 (2018).
20. Kim, S. M. et al. Superior toughness and fast self-healing at room temperature engineered by tranparent elastomers. *Adv. Mater.* **30**, 1705145 (2018).
21. Eom, Y. et al. Mechano-responsive hydrogen-bonding array of thermoplastic polyurethane elastomer captures both strength and self-healing. *Nat. Commun.* **12**, 621 (2021).
22. Park, H. et al. Toughening self-healing elastomer crosslinked by metal–ligand coordination through mixed counter anion dynamics. *Nat. Commun.* **14**, 5026 (2023).
23. Wu, X. et al. Dual-hard phase structures make mechanically tough and autonomous self-healable polyurethane elastomers. *Chem. Eng. J.* **454**, 140268 (2023).
24. Sarma, R. J., Otto, S. & Nitscheke, J. R. Disulfides, imines, and metal coordination within a single system: interplay between three dynamic equilibria. *Chem. Eur. J.* **13**, 9542 (2007).
25. Belengure, A., Friscic, T., Day, G. & Sanders, G. M. Solid-state dynamic combinatorial chemistry: reversibility and thermodynamic product selection in covalent mechanosynthesis. *Chem. Sci.* **2**, 696 (2011).
26. Azcunne, I. & Odriozola, I. Aromatic disulfide crosslinks in polymer systems: Self-healing, reprocessability, recyclability and more. *Eur. Polym. J.* **84**, 147 (2016).
27. Yan, X. et al. Quadruple H-Bonding cross-linked supramolecular polymeric materials as substrates for stretchable, antitearing, and self-healable thin film electrodes. *J. Am. Chem. Soc.* **140**, 5280–5289 (2018).
28. Mackanic, D. et al. Decoupling of mechanical properties and ionic conductivity in supramolecular lithium ion conductors. *Nat. Commun.* **10**, 5384 (2019).
29. You, I. et al. Artificial multimodal receptors based on ion relaxation. *Science* **370**, 961–965 (2020).

30. Son, D. et al. An integrated self-healable electronic skin system fabricated via dynamic reconstruction of a nanostructured conducting network. *Nat. Nanotechnol.* **13**, 1057–1065 (2018).
31. Tee, B. K., Wang, C., Allen, R. & Bao, Z. An electrically and mechanically self-healing composite with pressure- and flexion-sensitive properties for electronic skin applications. *Nat. Nanotechnol.* **7**, 825–832 (2012).
32. Tian, K., Pan, Q., Deng, H. & Fu, Q. Shear induced formation and destruction behavior of conductive networks in nicekl/polyurethane composites during strain sensing. *Compos. Part A Appl. Sci. Manuf.* **130**, 105757 (2020).
33. Xavier, M. S. et al. Soft pneumatic actuators: a review of design, fabrication, modeling, sensing, control and applications. *IEEE Access* **10**, 59442–59485 (2022).
34. Na, H. et al. Hydrogel-based strong and fast actuators by electro-osmotic tugor pressure. *Science* **376**, 301–307 (2022).
35. Gangjee, A. et al. Design, synthesis, and X-ray crystal structure of a potent dual inhibitor of thymidylate synthase and dihydrofolate reductase as an antitumor agent. *J. Med. Chem.* **43**, 3837–3851 (2000).

Acknowledgements

This study was supported by the Nano & Material Technology Development Program through the National Research Foundation of Korea (NRF) funded by Ministry of Science and ICT (NRF grants RS-2024-00402972), the Wearable Platform Materials Technology Center 24 (WMC, Grant No. NRF-2022R1A5A6000846) and Global Bio-Integrated Materials Center (RS- 2024-00406240).

Author contributions

J.J., I.Y., and J.K. conceived and designed the experiments. J.J. synthesized and characterized the self-healing polymers. J.J., J.C., and H.K. performed mechanical testings of polymers. J.J., S.L., and W.L. fabricated sensors and grippers. J.J. and S.L. characterized sensors and soft robots. J.J., I.Y., and J.K. wrote the paper. All the authors discussed the results and commented on the manuscript. J.K. supervised the study.

Competing interests

The authors declare no competing interests.

Additional information

Supplementary information The online version contains supplementary material available at https://doi.org/10.1038/s41467-024-53957-0.

Correspondence and requests for materials should be addressed to Insang You or Jiheong Kang.

Peer review information *Nature Communications* thanks the anonymous, reviewer(s) for their contribution to the peer review of this work. A peer review file is available.